ARTICLE

Solid Nanotubes Comprising α-Fe_2O_3 Nanoparticles Prepared from Ferritin Protein

Xue Qu,[†] Nao Kobayashi,[†] and Teruyuki Komatsu[†,‡,*]

[†]Research Institute for Science and Engineering, Waseda University, 3-4-1 Okubo, Shinjuku-ku, Tokyo 169-8555, Japan, and [‡]PRESTO, Japan Science and Technology Agency (JST), 4-1-8 Honcho, Kawaguchi-shi, Saitama 332-0012, Japan

ABSTRACT Solid nanotubes comprising α-Fe_2O_3 nanoparticles were prepared from iron-storage protein ferritin. Their structure, magnetic properties, and photocatalytic activities were characterized. The initial ferritin nanotube precursors were fabricated using alternating layer-by-layer depositions of poly-L-arginine (PLA) and ferritin into a track-etched polycarbonate membrane (pore diameter, 400 nm) with subsequent dissolution of the template. The obtained uniform cylinders of (PLA/ferritin)$_3$ (outer diameter, 410 ± 14 nm) were calcinated at 500 °C under air, yielding reddish-brown iron oxide nanotubes. The one-dimensional hollow structure remained perfect, but its diameter, wall thickness, and maximum length were markedly diminished. Disappearance of the protein shell and the PLA layers were confirmed using IR and EDX spectroscopy. Subsequent SEM, TEM, and XPS measurements showed that the tubular walls comprise fine α-Fe_2O_3 nanoparticles with a 5 nm diameter. These α-Fe_2O_3 nanotubes demonstrated superparamagnetic properties with a blocking temperature of 37 K and efficient photocatalytic activity for degradation of 4-chlorophenol.

KEYWORDS: α-Fe_2O_3 · nanotube · ferritin · nanoparticle · photocatalysis

One-dimensional (1-D) cylindrical hollow structures, so-called nanotubes, composed of metal oxides have attracted considerable attention because of their potential applications for sensors, magnetics, electronics, catalysis, and optics.[1−4] Hematite (α-Fe_2O_3) is the most stable iron oxide under ambient conditions and has *n*-type semiconducting properties with a small band gap of 2.2 eV. In terms of both scientific and technological importance, much effort has been made in synthesizing α-Fe_2O_3 nanotubes,[5,6] which can be exploited as a gas sensor,[7,8] anode material for lithium-ion battery,[7] soft magnet,[9,10] and photocatalysis.[10] A successful procedure used to prepare the α-Fe_2O_3 nanotubes is template synthesis using an anodic aluminum oxide (Al_2O_3) membrane (thickness: 60 μm). Xu *et al.* first fabricated beautiful nanotube arrays composed of 10-nm α-Fe_2O_3 particles by pyrolysis of $Fe(acac)_3$.[5] Similar nanotubes were also produced by Chen *et al.*, who used thermal decomposition of $Fe(NO_3)_3$.[7] Zhan and Wong prepared $Fe(OH)_3$ films onto the channel walls using a U-tube cell and converted them to the α-Fe_2O_3 nanotubes.[10] In all cases, the porous hard templates were removed by chemical etching in aqueous NaOH, a strong basic solution.

We recently demonstrated the supramolecular synthesis of various protein nanotubes using an alternating layer-by-layer (LbL) assembly of negatively charged proteins and positively charged poly-L-arginine (PLA) into a track-etched polycarbonate (PC) membrane with subsequent dissolution of the template in organic solvent.[11,12] Ferritin (M_w = 460 kDa) is a cage-protein with 12 nm diameter. It can store 4500 iron atoms within the shell to create a fine 6-nm ferrihydrite core.[13,14] This ideal biomolecular architecture is stimulating efforts to develop the new field of ferritin-based nanomaterials.[15]

In this paper, we report for the first time the synthesis and structure of solid nanotubes comprising α-Fe_2O_3 nanoparticles prepared from ferritin. The unique hematite tubules that were obtained show superparamagnetic properties and good photocatalytic activity.

RESULTS AND DISCUSSION

Synthesis and Structure of α-Fe_2O_3 Nanotubes. The initial ferritin nanotube precursors were prepared by LbL assembly technique using nanoporous PC membrane.[11,12] Three-cycle injections of the poly-L-arginine (PLA) solution followed by the ferritin solution into the PC template (pore diameter, D_p = 400 nm) using a syringe pump yielded multilayered thin-films on the pore walls. The obtained hybrid membrane was then im-

*Address correspondence to teruyuki@waseda.jp.

Received for review December 22, 2009 and accepted February 09, 2010.

Published online February 18, 2010. 10.1021/nn901879d

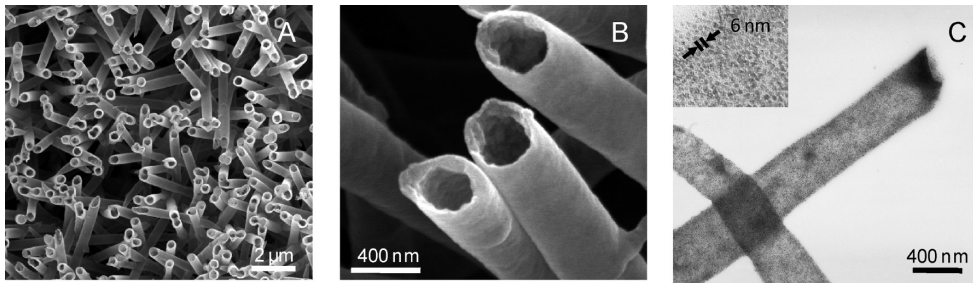

Figure 1. Electron microscopy images of (PLA/ferritin)$_3$ nanotubes prepared using a 400 nm porous PC template: (A,B) SEM and (C) TEM images.

mersed into *N,N*-dimethylformamide to dissolve the PC framework. The precipitates were quickly freeze-dried, yielding a pale-yellow powder of (PLA/ferritin)$_3$ nanotubes. From SEM measurements, the outer diameter and wall thickness of the tubules were determined respectively as 410 ± 14 and 61 ± 5 nm (Figure 1A,B). The maximum cylinder length (*ca.* 9 μm) corresponded to the membrane pore depth. If we assume a six-layered model of the tubular wall, in which each ferritin layer has single-protein thickness of 12 nm, then one PLA layer is estimated as 8.3 nm. This value appears to be somewhat thick, but it is still within the previously reported results of polyelectrolyte thin-films deposited into the nanoporous membrane under pressure conditions.[16,17] Later TEM observations of the dried sample showed dark images of the nanotubes because of the iron oxide cores in ferritin (Figure 1C). High-magnification pictures clearly exhibited the individual iron oxide dot of 6 nm.

To eliminate the protein shells and the polyelectrolyte layers from the (PLA/ferritin)$_3$ nanotubes, we conducted heat treatment under air. Calcination of the ferritin nanotubes at 500 °C for 4 h yielded reddish-brown powder (Scheme 1). The SEM and TEM measurements revealed that the 1-D hollow structure of the tubules was retained perfectly, but considerable shrinkage of the morphology was observed: 211 ± 8 nm outer diameter, 29 ± 3 nm wall thickness, and *ca.* 5 μm tube length (Figure 2). Careful inspections of the microscope images revealed that the cylindrical wall was composed of fine nanoparticles with a 5 nm diameter (Figure 2C); these grains must have originated from the iron oxide core of ferritin. Another method to remove the protein shell, enzymatic digestion with protease,[18] was not useful. After digestion of the (PLA/ferritin)$_3$ nanotubes using protease (Pronase), we found no tubular structure in the product.

Complete disappearance of the protein shells and PLA layers after calcination were confirmed using FT-IR and energy dispersive X-ray (EDX) spectroscopies. In an FT-IR spectrum of the (PLA/ferritin)$_3$ nanotubes, a typical protein amide I band (mainly attributed to C═O stretching vibrations) and an amide II band (C−N stretching coupled with N−H bending vibrations) were visible respectively at 1653 and 1547 cm^{-1} (Figure 3).[19] In marked contrast, the burned nanotubes showed no IR absorption in this region. Subsequent EDX spectroscopy also elucidated that the N and S peaks based on the polypeptides faded away after burning (Figure 4). Protein nanotubes prepared using human serum albumin (HSA) instead of ferritin—(PLA/HSA)$_3$ nanotubes—were evaporated entirely by the identical heat treatment. No residue such as amorphous carbon was left in the crucible. On the basis of these results, it can be concluded that the calcination of the (PLA/ferritin)$_3$ nanotubes at 500 °C for 4 h completely eliminates the protein cages and the polyelectrolyte glues, thereby yielding solid nanotubes comprising very fine iron oxide nanoparticles that are connected mutually at points of contact. In fact, combustion at 700 °C yielded rugged nanotubes composed of thermally fused iron oxides of *ca.* 20 nm diameter.

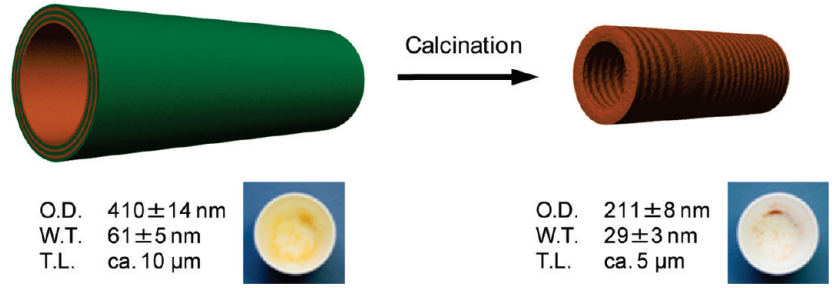

Scheme 1. Calcination of (PLA/ferritin)$_3$ nanotubes to yield iron oxide nanotubes: O.D., outer diameter; W.T., wall thickness; T.L., tube length. Photographs: lyophilized (PLA/ferritin)$_3$ pale-yellow nanotubes in a crucible (left) and calcinated iron oxide nanotubes in reddish-brown color (right).

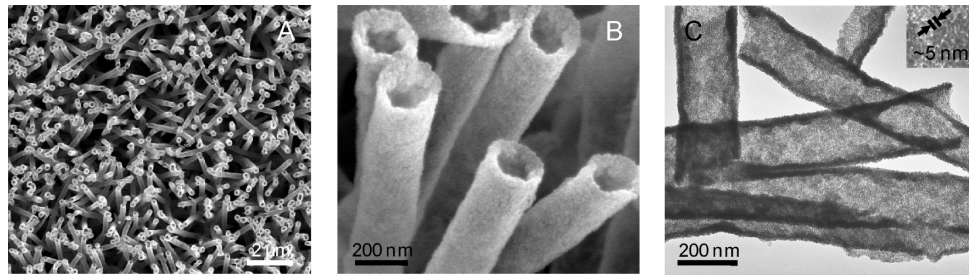

Figure 2. Electron microscopy images of calcinated nanotubes prepared from (PLA/ferritin)$_3$ nanotubes with an outer diameter of *ca.* 400 nm (shown in Figure 1): (A,B) SEM and (C) TEM images.

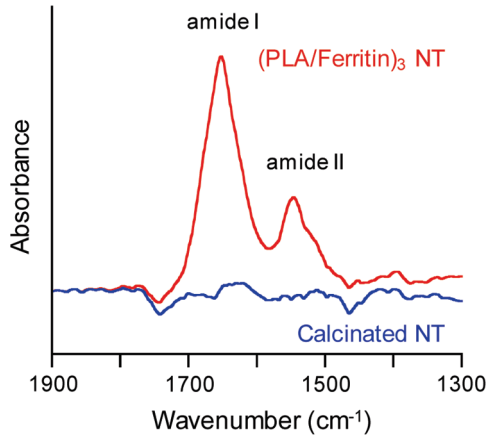

Figure 3. IR spectra of (PLA/ferritin)$_3$ nanotubes (red) and calcinated nanotubes (blue).

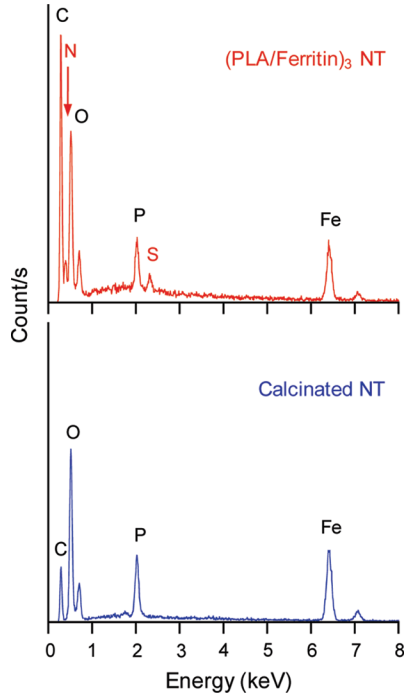

Figure 4. EDX spectra of (top) (PLA/ferritin)$_3$ nanotubes and (bottom) calcinated nanotubes.

The wide-survey X-ray photoelectron spectroscopy (XPS) pattern of the calcinated nanotubes exhibited predominant peaks attributed to O and Fe, but showed no N1s peak at 399 eV (data not shown).[20] That fact also implies that all polypeptide components were eliminated by the heating. The spectral shape and binding energies of the significant peaks of $Fe2p_{2/3}$ (711.0 eV) and $Fe2p_{1/2}$ (724.4 eV) show good agreement with previously reported data of the α-Fe_2O_3 nanotubes[8] and crystals[20] (Figure 5). Consequently, we reasoned that our iron oxide nanotubes comprise numerous fine α-Fe_2O_3 grains; they are expected to show properties combining nanoparticles and cylindrical hollows.

Magnetic Properties. In general, magnetic behaviors of nanomaterials differ from those of the corresponding bulk form because of their finite-size effect in nanometer scale. We measured the temperature-dependent magnetic susceptibility ($\chi = M/H$) of our α-Fe_2O_3 nanotubes using a superconducting quantum interference device (SQUID) in an applied magnetic field (H) of 100 or 500 Oe from 5 to 300 K using field-cooling (FC) or zero-field-cooling (ZFC) procedures (Figure 6). Bulk α-Fe_2O_3 normally shows a sharp magnetic phase transition at 260 K (T_M)—the so-called Morin temperature—at which a drastic decline of magnetization is observed from the canted ferromagnetic phase (above T_M) to the antiferromagnetically ordered state (below T_M).[21,22] As expected, the magnetic properties of our α-Fe_2O_3 nanotubes differed greatly from that of bulk α-Fe_2O_3; the ZFC curves showed a well-defined peak at 37 K, namely blocking temperature (T_B). At 5 K, the magnetic moments are blocked to oscillate across the anisotropy barrier because of insufficient thermal energy. As the temperature increased, the spins are activated, leading to an increase in χ(ZFC), and the α-Fe_2O_3 nanotubes show superparamagnetic performance. Similar magnetic behavior was found in the ZFC curves of hydrothermally synthesized α-Fe_2O_3 nanotubes,[10] α-Fe_2O_3 nanocubes,[23] and mesoporous α-Fe_2O_3 with disordered walls.[22] Nevertheless, in our case, it is noteworthy that the unique temperature independence of the FC curve was observed below T_B, especially under 100 Oe. This contrasts with observations in ferritin[24] and other α-Fe_2O_3 nanostructures where the χ(FC) increases continuously with falling temperature.[9,10,22,23] This result suggests the presence of a strong intratubular interaction of magnetic ordering in our hematite cylinders.

The field-dependence curves of the α-Fe_2O_3 nanotubes at 5 K displayed a small hysteresis loop with coer-

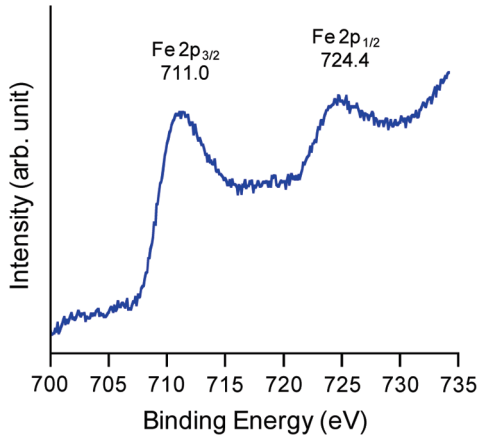

Figure 5. XPS spectrum of α-Fe_2O_3 nanotubes.

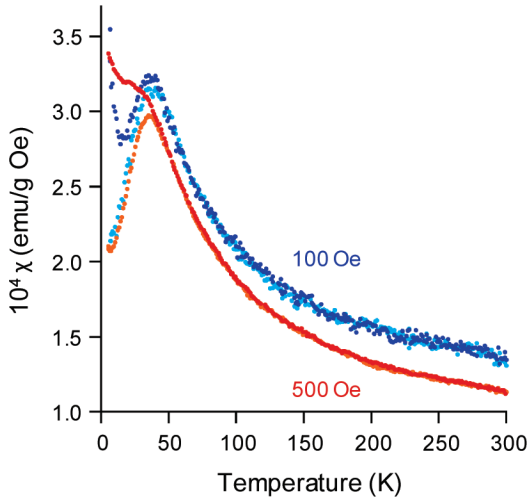

Figure 6. Temperature-dependent magnetic susceptibility (χ = *M*/*H*) of α-Fe_2O_3 nanotubes at two applied fields (100 and 500 Oe). Blue and light-blue lines represent field-cooling (FC) and zero-field-cooling (ZFC) curves at 100 Oe. The red and orange lines are FC and ZFC curves at 500 Oe.

cive force (H_c) of 330 Oe and remanent magnetization of 0.28 emu/g, indicative of weak ferromagnetic behavior as a soft magnet (Figure 7). No saturation of the magnetization was found up to the maximum applied field. This superparamagnetic property resembles those of other α-Fe_2O_3 nanostructures.[9,10,25] Zhou and Wong reported a H_c of 245 Oe for α-Fe_2O_3 nanotubes[10] and Tang *et al*. demonstrated a H_c of 187 Oe for α-Fe_2O_3 nanorods.[25] The 1-D morphology can increase the shape anisotropy compared to the spherical particles. It presumably enhances the magnetic coercive force.

Photocatalytic Activity. Semiconductor-assisted photooxidation by solar energy is a reasonable method for converting organic pollutants into harmless molecules. We investigated the catalytic performance of α-Fe_2O_3 nanotubes by photosensitized degradation of 4-chlorophenol (4CP) using practically weak visible light (40 mW cm^{-2}) in the presence of H_2O_2 as an electron acceptor.[26] For comparison, commercial bulk α-Fe_2O_3 powder was used as a control. The α-Fe_2O_3 nanotubes were suspended in water (1.5 mL) by brief soni-

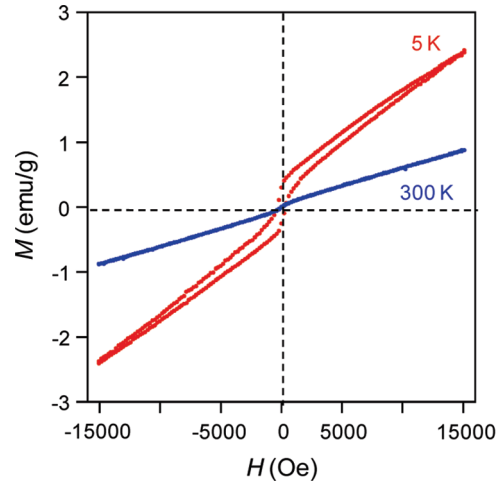

Figure 7. Magnetic hysteresis loop of α-Fe_2O_3 nanotubes at 5 K (red line) and 300 K (blue line).

cation for 2 min. The tubes were sufficiently stable to endure sonication, as confirmed by SEM (Supporting Information Figure S1). The bulk α-Fe_2O_3 diameter was estimated as 400 ± 85 nm using dynamic light scattering measurements. The aqueous dispersion of the α-Fe_2O_3 nanotubes showed a broad UV−vis absorption band with a maximum at 386 nm, which was almost identical to those of α-Fe_2O_3 crystals (Supporting Information Figure S2).[10] Marusak *et al*. assigned the absorption peak around 385 nm as a charge-transfer band of $O^{2-} \rightarrow Fe^{3+}$.[27]

The concentration change of 4CP in the sample dispersion was assayed by measuring the absorption intensity at 280 nm. In the dark, 4CP was not decomposed in every case whether in the presence or absence of α-Fe_2O_3 (nanotube or bulk) over 7 h (Figure 8). In contrast, under the exposure of visible light (340−800 nm), significant decreases of the 4CP concentration were observed in dispersions with the α-Fe_2O_3 nanotubes and bulk α-Fe_2O_3, although no degradation was found in the control solution. In particular, the α-Fe_2O_3 nanotubes exhibited more efficient photocatalytic activity than bulk α-Fe_2O_3 did. With band gap illumination, electron−hole pairs are formed on the tube surfaces. The hole is trapped by H_2O to produce hydroxyl radical ($OH^{\bullet}$), which is responsible for the oxidation of 4CP. On the other hand, the fate of the electron occurs *via* (i) trapping by H_2O_2, which also generates $OH^{\bullet}$, and (ii) trapping by the surface Fe^{3+}, which forms Fe^{2+} leading to Fenton reaction.[26] The $OH^{\bullet}$ is produced in both pathways favored at acidic conditions. Notably, the photodegradation rate was accelerated after 50 min in the dispersion with the α-Fe_2O_3 nanotubes (Figure 8). Similar but less acceleration was also apparent in the bulk α-Fe_2O_3 system, which is likely to result from a decrease of the solution pH. In fact, the initial pH 6.5 of the mixture with the α-Fe_2O_3 nanotubes or bulk α-Fe_2O_3 slowly declined to pH 4.5 at the end of the reaction because HCl is generated along with the decomposition of

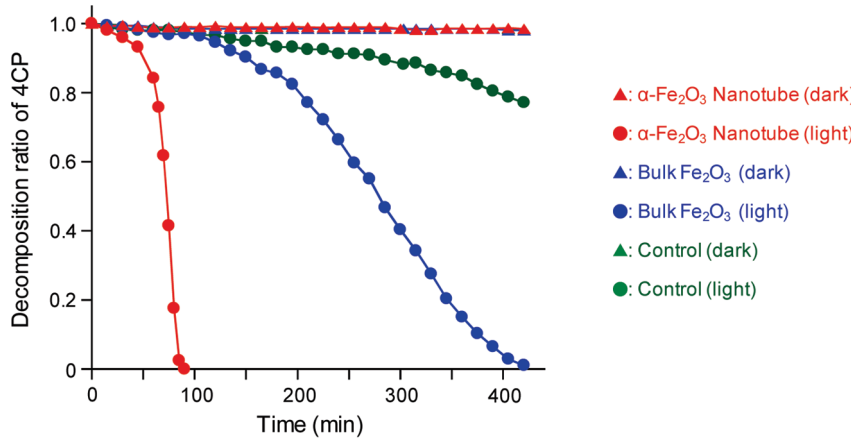

Figure 8. Photodegradation of 4CP in aqueous solution with H_2O_2 under visible light irradiation.

4CP.[26] This result is broadly similar to that described in the previous report of Kiwi *et al.*[28] Modest photooxidation observed in the control solution without catalyst under the light is probably caused by slight overlapping of the absorption edge of 4CP and the irradiation light around 300 nm. The superior photocatalytic activity of the α-Fe_2O_3 nanotubes can be attributed to the large surface area based on the 1-D hollow structure composed of numerous α-Fe_2O_3 nanoparticles with a 5 nm diameter. The surface area of the nanotube (outer diameter, 211 nm) is estimated to be at least 7-fold larger than that of 400-nm spherical particle based on the geometrical model.

CONCLUSIONS

Results of this study show that the heat treatment of the rolled sandwiches of ferritin protein— (PLA/ferritin)$_3$ nanotubes—produced solid nanotubes comprising uniform α-Fe_2O_3 nanoparticles. The polypeptide components had disappeared completely, thereby the whole morphology was shrunk almost to half. The tube walls comprised fine spherical α-Fe_2O_3 grains of 5 nm diameter. This method, which requires only aqueous solutions of the materials, is an extremely green process: it is environmentally friendly. The obtained α-Fe_2O_3 nanotubes exhibited superparamagnetic properties and efficient catalytic activity for photodegradation of 4CP pollutant. Our results suggest that apoferritins including other metal ions or semiconductors can enable us to create different nanotubes comprising desired metal oxide nanoparticles smaller than 5 nm. For instance, Co_3O_4 nanotubes prepared from Co_3O_4 core apoferritin might conceivably be exploited for lithium-ion battery application. The TiO_2 nanotubes made from $Ti(OH)_3$ core apoferritin are useful for various band gap materials.

EXPERIMENTAL SECTION

Materials and Apparatus. Ferritin from equine spleen and poly-L-arginine hydrochloride (PLA, M_w: *ca.* 70 000) were purchased from Sigma-Aldrich Co. The ferritin was dialyzed for 12 h at 4 °C against 10 mM sodium phosphate buffer (PB) solution (pH 7.0, 10 mM) prior to use. Bulk α-Fe_2O_3 powder (99.9%) was purchased from Wako Pure Chemical Industries, Ltd. The water was deionized (18.2 MΩ · cm) using water purification systems (Elix UV and Simpli Lab-UV; Millipore Corp.). The UV−vis absorption spectra were obtained using a UV−visible spectrophotometer (8453; Agilent Technologies Inc.) equipped with a temperature control unit (89090A; Agilent Technologies Inc.).

Template Synthesis of Ferritin Nanotubes. The ferritin nanotube precursors were synthesized according to our previously reported procedure.[11,12] The PB solution (pH 7.0, 10 mM, 10 mL) of PLA (1 mg/mL) containing 0.1 M NaCl was filtered through a track-etched polycarbonate (PC) membrane (isopore membrane, 25 mm, pore diameter (D_p) 400 nm; Millipore Corp.) (0.25 mL/min) using a syringe pump (PHD-2000; Harvard Apparatus). Excess PLA absorbed on the pore wall was removed by water filtration (10 mL, 1.0 mL/min), followed by drying under reduced pressure for 10 min. Then the PB solution (pH 7.0, 10 mM, 10 mL) of ferritin (1 mg/mL) was filtered through the membrane (0.5 mL/min) to deposit the second layer of negatively charged ferritin. After washing with water (10 mL, 1.0 mL/min), the membrane was dried again *in vacuo* for 10 min. These pressure infiltrations were repeated for three cycles. The PC membrane surface was wiped gently using a cotton swab and dried in an automatic low-humidity chamber (Super Dry; Toyo Living Co. Ltd., Japan) for 12 h (humidity ≤1%). To isolate the cylindrical cores from the PC template, the membrane was immersed into an *N,N*-dimethylformamide solution. The precipitated pieces were rapidly freeze-dried *in vacuo*, yielding uniform (PLA/ferritin)$_3$ nanotubes as a pale-yellow powder.

Heat Treatment of Ferritin Nanotubes. The lyophilized (PLA/ferritin)$_3$ nanotubes (*ca.* 0.2 mg) were calcinated in a crucible under air within a muffle furnace (FP32; Yamato Scientific Co. Ltd.). The temperature was gradually increased to 500 °C during 1 h, maintained for 4 h, and decreased to room temperature over a period of 2 h. The obtained reddish-brown powder (α-Fe_2O_3 nanotubes) was stored in an automatic low-humidity chamber (humidity ≤1%).

Scanning Electron Microscopy (SEM) and Transmission Electron Microscopy (TEM) Observations. For SEM measurements of the nanotubes, the sample was fixed on double-sided conductive carbon tape and sputter-coated with Pd−Pt using an ion sputter (E-1045; Hitachi Ltd.). The SEM observations were conducted using a scanning electron microscope (S-4300; Hitachi Ltd.) with an accelerating voltage of 10 kV. To determine an average size of the outer diameter and wall thickness, at least 50 different nanotubes were evaluated. The energy dispersive X-ray (EDX) spectra were measured using a detecting unit (HIT S3000N; EDAX Inc.) attached to scanning electron microscope (S-3000N; Hitachi Ltd.).

For TEM observations, 6 μL of the aqueous dispersion of the nanotubes was dropped onto an elastic carbon-coated copper grid (100 mesh; Okenshoji Co. Ltd.) and air-dried at room temperature with no staining. The grid's surface was hydrophilized in advance by glow charge using a hydrophilic treatment device (HDT-400; JEOL Datum). These specimens were observed using a transmission electron microscope (JEM-1011; JEOL) with accelerating voltage of 100 kV.

Enzymatic Digestions with Protease. The $(PLA/ferritin)_3$ nanotubes were dispersed in pure water (1.5 mL) and protease (Pronase; Roche Diagonostics GmbH) was added to the solution ([Pronase] = 1 mg/mL). The mixture was incubated for 4 h at 25 °C and freeze-dried *in vacuo*. The digested nanotube morphology was observed using SEM.

FT-IR Spectroscopy. For FT-IR measurements, small KBr discs were prepared with the powder of nanotubes. The spectra at 4 cm^{-1} resolution were recorded using an FT-IR spectrophotometer (FT/IR-4200; Jasco Inc.).

X-ray Photoelectron Spectroscopy (XPS). For this study, XPS of the calcinated nanotubes was performed with an X-ray photoelectron spectrometer (JPS-9010TR; JEOL) using Mg Kα X-ray radiation. The powder sample was mounted on stainless plate with carbon tape. Charging of the XPS spectra was corrected carefully using adventitious carbon (binding energies 284.6 eV) as a reference.

Superconducting Quantum Interference Device (SQUID). Magnetization measurements were conducted using a magnetic property measurement system (MPMS-7; Quantum Design) SQUID magnetometer at temperatures of 5−300 K at an applied field of 100 or 500 Oe. Magnetization *versus* applied field measurements were obtained using *H* values of −15 000 to 15 000 Oe. Powder of the α-Fe_2O_3 nanotubes was loaded into a gelatin capsule and fixed with soft paper. The sample was then held into a polyethylene drinking straw, which was attached to the sample rod of the MPMS apparatus.

Photodegradation of 4-Chlorophenol. The α-Fe_2O_3 nanotubes (75 μg) were suspended into water (1.5 mL) by brief sonication for 2 min. The tubes were sufficiently stable to endure sonication. The obtained pale-red dispersion was transferred to a quartz cuvette (optical path length: 10 mm), and 4-chlorophenol (4CP) and H_2O_2 were added ([4CP] = 0.3 mM, [H_2O_2] = 10 mM). Prior to light irradiation, the mixture was stirred magnetically in the dark for 2 h at 22 °C for pre-equilibration. The sample cuvette was then exposed to visible light from a 150 W xenon arc lamp (Hamamatsu Photonics KK) in conjunction with UV34 and HA30 filters (Hoya Corp.) to eliminate the UV light and excess heating. The dispersion was conducted by magnetic stirring under air at 22 °C; the filtered light intensity at the sample cuvette was 40 mW cm^{-2}. Concentration of 4CP in the solution was assayed by measuring the UV absorbance at 280 nm. Comparison experiments were performed using commercial bulk α-Fe_2O_3 or without catalyst under the same conditions. The size distribution of the bulk α-Fe_2O_3 in water was determined using dynamic light scattering measurements (Zetasizer Nano; Malvern Instruments, Ltd.).

Acknowledgment. This work was supported by PRESTO "Control of Structure and Functions" JST, Grant-in-Aid for Scientific Research for Priority Areas (Coordination Programming) (area 2107) from MEXT Japan, and Grant-in-Aid for Scientific Research (B) (No. 20350058) from JSPS. Skillful experiments on photooxidations conducted by Ms. Hiromi Terada are gratefully acknowledged.

Supporting Information Available: SEM image of α-Fe_2O_3 nanotubes after brief sonication (Figure S1), UV−vis absorption spectrum of α-Fe_2O_3 nanotubes in water (Figure S2). This material is available free of charge *via* the Internet at http://pubs.acs.org.

REFERENCES AND NOTES

1. Xia, Y.; Yang, P.; Sun, Y.; Wu, Y.; Mayers, B.; Gates, B.; Yin, Y.; Kim, F.; Yan, H. One-Dimensional Nanostructures: Synthesis, Characterization, and Applications. *Adv. Mater.* **2003**, *15*, 353–389.
2. Rao, C. N. R.; Nath, M. Inorganic Nanotubes. *Dalton Trans.* **2003**, *1*, 1–24.
3. Ghicov, A.; Schmuki, P. Self-Ordering Electrochemistry: A Review on Growth and Functionality of TiO_2 Nanotubes and Other Self-Aligned MO_x Structures. *Chem. Commun.* **2009**, 2791–2808.
4. Kogiso, M.; Zhou, Y.; Shimizu, T. Instant Preparation of Self-Assembled Metal−Complexed Lipid Nanotubes that Act as Templates To Produce Metal Oxide Nanotubes. *Adv. Mater.* **2007**, *19*, 242–246.
5. Shen, X.-P.; Liu, H.-J.; Pan, L.; Chen, K.-M.; Hong, J.-M.; Xu, Z. An Efficient Template Pathway to Synthesis of Ordered Metal Oxide Nanotube Arrays Using Metal Acetylacetonates as Single-Source Molecular Precursors. *Chem. Lett.* **2004**, *33*, 1128–1129.
6. Jia, C.-J.; Sun, L.-D.; Yan, Z.-G.; You, L.-P.; Luo, F.; Han, X.-D.; Pang, Y.-C.; Zhang, Z.; Yan, C.-H. Single-Crystalline Iron Oxide Nanotubes. *Angew. Chem., Int. Ed.* **2005**, *44*, 4328–4333.
7. Chen, J.; Xu, L.; Li, W.; Gou, X. α-Fe_2O_3 Nanotubes in Gas Sensor and Lithium-Ion Battery Applications. *Adv. Mater.* **2005**, *17*, 582–586.
8. Sun, Z.; Yuan, H.; Liu, Z.; Han, B.; Zhang, X. A Highly Efficient Chemical Sensor Material for H_2S: α-Fe_2O_3 Nanotubes Fabricated Using Carbon Nanotubes Templates. *Adv. Mater.* **2005**, *17*, 2993–2997.
9. Liu, L.; Kou, H.-Z.; Mo, W.; Liu, H.; Wang, Y. Surfactant-Assisted Synthesis of α-Fe_2O_3 Nanotubes and Nanorods with Shape-Dependent Magnetic Properties. *J. Phys. Chem. B* **2006**, *110*, 15218–15223.
10. Zhou, H.; Wong, S. S. A Facile and Mild Synthesis of 1-D ZnO, CuO, and α-Fe_2O_3 Nanostructures and Nanostructured Arrays. *ACS Nano* **2008**, *2*, 944–958.
11. Qu, X.; Lu, G.; Tsuchida, E.; Komatsu, T. Protein Nanotubes Comprised of an Alternate Layer-by-Layer Assembly Using a Polycation as an Electrostatic Glue. *Chem.—Eur. J.* **2008**, *14*, 10303–10308.
12. Qu, X.; Komatsu, T. Molecular Capture in Protein Nanotubes. *ACS Nano* **2010**, *4*, 563–573.
13. Hoare, R. J.; Harrison, P. M.; Hoy, T. G. Structure of Horse-Spleen Apoferritin at 6 Å Resolution. *Nature* **1975**, *225*, 653–654.
14. Ford, G. C.; Harrison, P. M.; Rice, D. W.; Smith, J. M. A.; Treffry, A.; White, J. L.; Yariv, J. Ferritin: Design and Formation of an Iron-Storage Molecule. *Phil. Trans. R. Soc. London* **1984**, *B 304*, 551–565.
15. Yamashita, I. Fabrication of a Two-Dimensional Array of Nanoparticles Using Ferritin Molecule. *Thin Solid Films* **2001**, *398*, 12–18.
16. Ai, S.; Lu, G.; He, Q.; Li, J. Highly Flexible Polyelectrolyte Nanotubes. *J. Am. Chem. Soc.* **2003**, *125*, 11140–11141.
17. Alem, H.; Blondeau, F.; Glinel, K.; Demoustier-Champagne, S.; Jonas, A. M. Layer-by-Layer Assembly of Polyelectrolytes in Nanopores. *Macromolecules* **2007**, *40*, 3366–3372.
18. Borodina, T.; Markvicheva, E.; Kunizhev, S.; Möhwald, H.; Sukhorukov, G. B.; Kreft, O. Controlled Release of DNA from Self-Degrading Microcapsules. *Macromol. Rapid Commun.* **2007**, *28*, 1894–1899.
19. Byler, D. M.; Sui, H. Examination of the Secondary Structure of Proteins by Deconvoluted FTIR Spectra. *Biopolymers* **1986**, *25*, 469–487.
20. McIntyre, N. S.; Zetaruk, D. G. X-ray Photoelectron Spectroscopic Studies of Iron Oxides. *Anal. Chem.* **1977**, *49*, 1521–1529.
21. Morin, F. J. Magnetic Susceptibility of α-Fe_2O_3 and α-Fe_2O_3 with Added Titanium. *Phys. Rev.* **1950**, *78*, 819–820.
22. Jiao, F.; Harrison, A.; Jumas, J.-C.; Chadwick, A. V.; Kockelmann, W.; Bruce, P. G. Ordered Mesoporous Fe_2O_3 with Crystalline Walls. *J. Am. Chem. Soc.* **2006**, *128*, 5468–5474.
23. Wang, S.-B.; Min, Y.-L.; Yu, S.-H. Synthesis and Magnetic Properties of Uniform Hematite Nanocubes. *J. Phys. Chem. C* **2007**, *111*, 3551–3554.

24. Gider, S.; Awschalom, D. D.; Douglas, T.; Mann, S.; Chaparala, M. Classical and Quantum Magnetic Phenomena in Natural and Artificial Ferritin Proteins. *Sciences* **1995**, *268*, 77–80.
25. Tang, B.; Wang, G.; Zhuo, L.; Ge, J.; Cui, L. Facile Route to α-FeOOH and α-Fe_2O_3 Nanorods and Magnetic Property of α-Fe_2O_3 Nanorods. *Inorg. Chem.* **2006**, *45*, 5196–5200.
26. Pera-Titus, M.; García-Molina, V.; Baños, M. A.; Giménez, J.; Esplugas, S. Degradation of Chlorophenols by Means of Advanced Oxidation Process: A General Review. *Appl. Catal. B: Environ.* **2004**, *47*, 219–256.
27. Marusak, L. A.; Messier, R.; White, W. B. Optical Absorption Spectrum of Hematite, α-Fe_2O_3 Near IR to UV. *J. Phys. Chem. Solids* **1980**, *41*, 981–984.
28. Bandara, J.; Klehm, U.; Kiwi, J. Raschig Ring-Fe_2O_3 Composite Photocatalyst Activate in the Degradation of 4-Chlorophenol and Orange II under Daylight Irradiation. *Appl. Catal. B: Environ.* **2007**, *76*, 73–81.